Icarus 252 (2015) 277–283

Contents lists available at ScienceDirect

Icarus

journal homepage: www.elsevier.com/locate/icarus

The Yarkovsky effect for 99942 Apophis

David Vokrouhlický [a,*], Davide Farnocchia [b], David Čapek [c], Steven R. Chesley [b], Petr Pravec [c], Petr Scheirich [c], Thomas G. Müller [d]

[a] Institute of Astronomy, Charles University, V Holešovičkách 2, CZ-180 00 Prague 8, Czech Republic
[b] Jet Propulsion Laboratory/California Institute of Technology, 4800 Oak Grove Drive, Pasadena, CA 91109, USA
[c] Astronomical Institute, Czech Academy of Sciences, Fričova 298, CZ-251 65 Ondřejov, Czech Republic
[d] Max-Planck-Institut für extraterestrische Physik, Giessenbachstrasse, Postfach 1312, D-85741 Garching, Germany

ARTICLE INFO

Article history:
Received 24 October 2014
Revised 4 January 2015
Accepted 14 January 2015
Available online 31 January 2015

Keywords:
Celestial mechanics
Asteroids, dynamics
Asteroids, rotation

ABSTRACT

We use the recently determined rotation state, shape, size and thermophysical model of Apophis to predict the strength of the Yarkovsky effect in its orbit. Apophis does not rotate about the shortest principal axis of the inertia tensor, rather its rotational angular momentum vector wobbles at an average angle of $\simeq 37°$ from the body axis. Therefore, we pay special attention to the modeling of the Yarkovsky effect for a body in such a tumbling state, a feature that has not been described in detail so far. Our results confirm that the Yarkovsky effect is not significantly weakened by the tumbling state. The previously stated rule that the Yarkovsky effect for tumbling kilometer-size asteroids is well represented by a simple model assuming rotation about the shortest body axis in the direction of the rotational angular momentum and with rotation period close to the precession period is confirmed. Taking into account uncertainties of the model parameters, as well as the expected density distribution for Apophis' spectral class, we predict the secular change in the semimajor axis is $(-12.8 \pm 3.6) \times 10^{-4}$ au/Myr (formal 1σ uncertainty). The currently available astrometric data for Apophis do not allow an unambiguous direct detection of the Yarkovsky effect. However, the fitted secular change in semimajor axis of $(-23 \pm 13) \times 10^{-4}$ au/Myr is compatible with the model prediction. We revise the Apophis' impact probability information in the second half of this century by extending the orbital uncertainty derived from the current astrometric data and by taking into account the uncertainty in the dynamical model due to the thermal recoil accelerations. This is done by mapping the combined uncertainty to the close encounter in 2029 and by determining the statistical weight of the known keyholes leading to resonant impact orbits. Whereas collision with the Earth before 2060 is ruled out, impacts are still possible from 2060 with probabilities up to a few parts in a million. More definitive analysis will be available after the Apophis apparition in 2020–2021.
© 2015 Elsevier Inc. All rights reserved.

1. Introduction

There are few orbits among near-Earth asteroids that would be more remarkable than that of 99942 Apophis as far as efforts of their future propagation are concerned. The interest in Apophis is naturally powered by the impact threat of this asteroid in the second half of this century. The study of Apophis' hazard has already benefited from significant observational efforts, including dedicated radar and optical astrometry observations and efforts in understanding possible biases or local systematic errors in optical astrometry. The most important aspect of the Apophis orbit is an extraordinarily close approach to the Earth in April 2029 that will have a hugely amplifying effect on the orbital uncertainty. As a result, predicting Apophis' future orbit requires forefront techniques in modeling even very tiny perturbations in order to ascertain the circumstances of the 2029 encounter. Thus the Apophis case shares the same strict accuracy requirements on the dynamical model as other asteroids with known possibility of far-future impacts, e.g., (29075) 1950 DA (Giorgini et al., 2002; Farnocchia and Chesley, 2014), (101955) Bennu (Milani et al., 2009; Chesley et al., 2014) and (410777) 2009 FD (Spoto et al., 2014). And yet for Apophis the impact hazard lies decades rather than centuries in the future, and so the need to solve the problem soon is higher.

While the "standard artillery" of gravitational perturbations, including the relativistic effects and perturbations from massive asteroids, is being used in these highly-demanding cases, it has been also recognized that the main factor of uncertainty in the dynamical model arises from our inability to accurately model the non-gravitational effects. Of these, the Yarkovsky effect (e.g.,

* Corresponding author.
E-mail address: vokrouhl@cesnet.cz (D. Vokrouhlický).

http://dx.doi.org/10.1016/j.icarus.2015.01.011
0019-1035/© 2015 Elsevier Inc. All rights reserved.

Bottke et al., 2006; Vokrouhlický et al., in press) plays the most important role. Chesley (2006) provides a very good introductory analysis of the Yarkovsky effect for Apophis, while more recent works of Giorgini et al. (2008), Chesley et al. (2009, 2010), and Farnocchia et al. (2013b) basically profit from longer astrometry databases, their better treatment or a more complete statistical analysis of the unknown parameters needed to estimate the strength of the Yarkovsky effect. Fundamental improvement in modeling the thermal accelerations is possible only after these parameters, such as the spin state, size, bulk density and surface thermal inertia, become well constrained.

Luckily, recent results from Pravec et al. (2014) and Müller et al. (2014) provide new physical constraints on Apophis, and the goal of this work is to use the new information for refinement of Apophis' orbit prediction, including revision of its future impact hazard. However, the solution is not as straightforward as it might look. This is because Pravec et al. (2014) found that Apophis does not rotate in the energetically lowest mode about the principal axis of inertia, but rather exhibits moderate tumbling. Since virtually all previous studies of the Yarkovsky effect assumed rotation about the principal body axis, we first need to describe in some detail how we deal with it in our approach[1] (Section 2). Next, we review the currently available astrometric observations of Apophis, both radar and optical, and apply up-to-date bias corrections to them. The dynamical model, completed by the thermal recoil accelerations, is then used for Apophis' orbit determination. This allows us to propagate its uncertainty to 2029, when Apophis encounters the Earth, and finally revise the impact threat in the second half of this century (Section 3).

2. Modeling the Yarkovsky effect for Apophis

The degenerate case of principal-axis rotation of an asteroid is characterized by a single (sidereal) rotation period in the inertial space. The general case of non-principal-axis rotation of an asymmetric body makes the description more complicated by involving two fundamental periods (e.g., Landau and Lifschitz, 1960). The first period, P_ψ, fully describes motion of the rotational angular momentum vector in the body fixed frame $\mathcal{B}$. Adopting the popular description of a transformation between the inertial space and $\mathcal{B}$ using a set of Euler angles (ϕ, θ, ψ) (see, e.g., Landau and Lifschitz, 1960; Kaasalainen, 2001), P_ψ sets the periodicity of the proper rotation angle ψ and the nutation angle θ. The second period, P_ϕ, describes the precession of $\mathcal{B}$ in the inertial space and it is needed to describe the Euler angle ϕ. Observationally, P_ψ and P_ϕ are the primary parameters set by the data analysis (e.g., Kaasalainen, 2001; Pravec et al., 2005). In a physical description of the rotation, they are however derived quantities depending on (i) the initial conditions, and (ii) parameters $I_a = A/C$ and $I_b = B/C$, where (A, B, C) are the principal moments of inertia. The fundamental periods P_ψ and P_ϕ could be obtained either by analytical formulas (e.g., Landau and Lifschitz, 1960, or Appendix B in Breiter et al., 2011, who use Andoyer canonical variables rather than Euler angles and their associated momenta). An alternative possibility is to use direct numerical integration of Euler kinematic equations (e.g., Landau and Lifschitz, 1960, or Appendix in Kaasalainen, 2001).

Apart from rotation, the asteroid undergoes also a translational motion in the inertial space. This is obviously its heliocentric motion, which is at the zero approximation (i.e., unperturbed orbit) characterized by the orbital period $P_{\rm orb}$. This brings a third independent fundamental period to the problem. The rotation-related periods P_ψ and P_ϕ would set up what is known as the diurnal component of the Yarkovsky effect, while the translation-related period $P_{\rm orb}$ would yield the corresponding seasonal component. However, since we derive a fully numerical solution of the Yarkovsky effect here, we do not need to adopt any particular split of the complete effect (which would be anyway difficult, especially when P_ψ is not significantly smaller than $P_{\rm orb}$ as in the Apophis case).

Before we proceed with some details of our solution, we note that the method used to solve the heat diffusion problem requires that the solution be periodic in time. Strictly speaking, this occurs only when $P_{\rm orb}$ is an integer multiple of both P_ψ and P_ϕ. Despite the fact that this may not be exactly satisfied, we can adopt the following approximate scheme enforcing the above mentioned periodicity[2]:

(i) we slightly change some of the parameters determining P_ψ and P_ϕ such that their ratio is a rational number;
(ii) we slightly change the semimajor axis of the heliocentric orbit such that both $P_{\rm orb}/P_\psi$ and $P_{\rm orb}/P_\phi$ are integer numbers.

A few comments are in order. The first step (i) is performed by a small redefinition of the I_a parameter within its uncertainty interval (for Apophis we use $|\delta I_a/I_a| \leqslant 0.5\%$, while the formal uncertainty of this quantity, as derived from observations, is $\simeq 10\%$; e.g., Pravec et al., 2014). There are obviously several solutions, so we choose those which then help to satisfy the second step (ii) with a minimum change of the orbital semimajor axis. Again for Apophis we use $|\delta a/a| \leqslant 1\%$. This is obviously more than the actual formal uncertainty in the semimajor axis determination. Henceforth, in a particular solution we redefine the solar constant, i.e., the solar radiation flux at a normalized heliocentric distance, such that the mean radiation flux over the true Apophis orbit is the same as the mean radiation flux over the "faked orbit" with a slightly redefined semimajor axis value. In order to justify our approach, we also compare at least two different variants of the solution (with two different rational values of P_ϕ/P_ψ). As expected, it turns out that the resulting mean semimajor axis change $\langle da/dt \rangle$, the most important effect in terms of orbit determination (e.g., Vokrouhlický et al., 2000), is insensitive to these details (see below).

Having discussed the issue of rotation modeling in some detail, we can now describe other components of our approach in a briefer way because they are rather standard (see, e.g., Čapek and Vokrouhlický (2005) or Čapek (2006) for more details). The asteroid shape is represented using a general polyhedron model with a typical number of surface facets ranging from hundreds to thousands. In the case of Apophis, the available model by Pravec et al. (2014) has 2024 surface facets. We consider the thermal history of each of the facets independently, not allowing a thermal communication between them by either conduction (e.g., Golubov and Krugly, 2012) or mutual thermal irradiation (e.g., Rozitis and Green, 2012, 2013). The space coordinate in the heat diffusion problem is simply vertical depth z below the facet, such that the space–time domain of the solution is in principle $(0, \infty) \times (0, P_{\rm orb})$. In reality though, we set an upper limit Z on the depth, such that the true domain of

[1] In passing, we note that our method is similar, but refines the one we used in the case of (4179) Toutatis (e.g., Čapek and Vokrouhlický, 2005; Vokrouhlický et al., 2005). At that time the need to compute thermal accelerations for tumbling objects was rather an academic exercise without having significant practical importance. With Apophis, and possibly other similar cases in the future, we believe this situation has changed.

[2] Note that we implicitly use the same trick also in the case of the Yarkovsky solution for asteroids rotating in the principal-axis mode by modifying the rotation period $P_{\rm rot}$ such that the ratio $P_{\rm orb}/P_{\rm rot}$ is integer. In this case, one can keep the orbit fixed and only slightly change the rotation period $P_{\rm rot}$ to satisfy the periodicity condition. Given typically short rotation periods of asteroids this usually involves a change in $P_{\rm rot}$ smaller than one per mille of its value, an insignificant change often within its uncertainty interval.

our solution becomes finite: $\mathcal{D} = (0, Z) \times (0, P_{\rm orb})$. The value of Z is set to be 15 times the estimated penetration depth $h_{\rm orb} = \sqrt{KP_{\rm orb}/2\pi\rho C}$ of the seasonal thermal wave, where K is the surface thermal conductivity, ρ is the surface density and C is the surface specific heat capacity.

Our solution is made explicit by setting conditions at the boundary $\partial\mathcal{D}$: (i) we impose $P_{\rm orb}$-periodicity of the solution, i.e., identify temperatures at time 0 and $P_{\rm orb}$ at any depth z, (ii) at depth Z we have a Neumann condition $(\partial T/\partial z)_{z=Z} = 0$, implying no further heat flux (i.e., an isothermal core of the body), and (iii) at the surface we have a non-linear Robin condition $\varepsilon\sigma T^4(z=0) - K(\partial T/\partial z)_{z=0} = E(t)$, where ε is the mean thermal emissivity, σ is the Stefan–Boltzmann constant and $E(t)$ is the absorbed solar radiative flux. The non-linearity of the surface condition requires an iterative method of solution.

Another non-trivial issue is a determination of $E(t)$ for non-convex asteroid shapes, since neighbor regions of the surface may sometimes shadow a given facet. Our code takes into account these shadowing effects by numerical ray-tracing of sunlight from the instantaneous direction to the Sun to the surface facet. If any other surface facet presents an obstacle, we set $E = 0$ at that moment of time. At present, though, the nominal shape model of Apophis as available from the lightcurve inversion technique is convex and does not involve such complications. We tested results from shape variants with slight non-convexities that are compatible with hull variations shown in Fig. 5 of Pravec et al. (2014), which provided resulting secular change in semimajor axis different from the nominal model by few percents at maximum. We also recall that we determine $E(t)$ for the whole timespan $P_{\rm orb}$ in the domain $\mathcal{D}$. This means our solution implicitly contains both diurnal and seasonal components of the Yarkovsky effect.

The heat diffusion equation itself is discretized according to a chosen grid on $\mathcal{D}$ and a finite difference method is adopted to obtain the solution. We use constant time-step dt, typically a small fraction of P_ϕ, and an exponentially increasing step in depth z with a surface value dz. The increase of the step in z is allowed by lessons drawn from a simplified analytical solution of the linearized heat diffusion problem that indicates an exponential decrease of the temperature difference with respect to the core with a penetration depth $h_\phi \simeq \sqrt{KP_\phi/2\pi\rho C}$. One may increment dz by a value $\exp(z/h_\phi)$ to compensate for the expected approximate temperature change. However, a z-dependent step would bring extra terms in the discretization scheme, so we opt for a simpler rule: $dz_j = dz\,\exp(\alpha j)$ for the step at the jth gridpoint with some value of a parameter α ($dz_0 = dz$; see, e.g., Brown and Matson, 1987). We typically use $\alpha \simeq 0.1$. We make sure that the chosen values grid steps, dt and dz, satisfy the von Neumann stability criterion. This is because we solve the heat diffusion equation using a simple explicit method described in Čapek (2006). The constant equilibrium temperature set on the whole grid in $\mathcal{D}$ is our starting condition, and we perform iterations until the temperature change at any gridpoint is less than 0.1%.

Once the heat diffusion solution converged, we know the surface temperature for each of the surface facets at any time along the revolution about the Sun. Assuming Lambertian thermal emission, the recoil acceleration $\Delta\mathbf{f}$ of the re-emitted radiation reads $\Delta\mathbf{f} = -(2/3)(\varepsilon\sigma T^4/mc)\Delta\mathbf{S}$, where c is the light velocity, m is the total mass of the body and $\Delta\mathbf{S}$ is the outward-oriented area of the facet. The contribution from all surface facets is summed-up to obtain a total thermal acceleration $\mathbf{f}(t) = \sum\Delta\mathbf{f}$ at a given time t along the orbit. These acceleration values are exported into a lookup table as a function of true anomaly that is used to compute $\langle da/dt\rangle$ from the Gauss planetary equations, and could be used for the orbit propagation of the asteroid.

With this approach we determine $\mathbf{f}$ along the unperturbed elliptical orbit rather then along the true heliocentric orbit of the asteroid. This is justified because the Yarkovsky effect is small enough that it does not directly produce a significant change in the orbital elements during the time span of interest. Of course, if the orbit undergoes a major change due to a planetary encounter, as is the case for Apophis in 2029, then the use of the unperturbed orbit becomes inappropriate and the lookup table must depend also on the orbital elements. Chesley et al. (2014) describe such an implementation approach, but as we show below, such sophistication is not needed for Apophis at present, but likely will be in the future.

At this moment we do not take into account the effects of surface roughness with a characteristic length scale smaller that the surface facets directly in our model. Rozitis and Green (2012, 2013) have shown that they could result in a slight increase of the Yarkovsky effect; this potential increase is empirically included in Section 2.2.

2.1. Parameters of the numerical solution for Apophis

In what follows, we use two thermal solutions A and B for Apophis along the lines explained above. Solution A has $I_{\rm a} = 0.61042$, while for solution B we set $I_{\rm a} = 0.60710$. In both cases we keep the nominal value $I_{\rm b} = 0.965$ from Pravec et al. (2014). Note that the currently nominal value for $I_{\rm a}$ is $0.61^{+0.11}_{-0.08}$ (3σ confidence interval; Pravec et al., 2014), so our A and B variants use $I_{\rm a}$ within the uncertainty interval of this parameter. The choices are made such that for case A we have $P_{\rm orb}/P_\phi = 280$ and $P_{\rm orb}/P_\psi = 29$ with $P_{\rm orb} = 319.5972$ day, and for case B $P_{\rm orb}/P_\phi = 288$ and $P_{\rm orb}/P_\psi = 30$ with $P_{\rm orb} = 328.5353$ day. The current Apophis orbit has, in fact, an orbital period of $\simeq 323.5$ day, so solution A corresponds to an orbit with somewhat smaller semimajor axis and vice versa for solution B. In quantitative terms we have $\delta a/a \simeq -0.8\%$ for solution A and $\delta a/a \simeq +1.0\%$ for solution B, assuming a to be the Apophis' current semimajor axis value. As mentioned above this is significantly more than the formal relative uncertainty in a but does not present a problem for our method. In each of solutions A and B we recalibrate the solar constant such that the mean influx of sunlight over these orbits is exactly the same as for the real orbit of Apophis.

We rescaled the polyhedral model of Pravec et al. (2014) such that it has a volume equal to a sphere with $D = 375$ m (Müller et al., 2014). For definiteness we adopted the following set of thermal parameters in our simulations: (i) the specific heat capacity $C = 680$ J/kg/K, (ii) both surface and bulk densities of 2 g/cm^3, (iii) the Bond albedo $A = 0.14$, and (iv) the thermal emissivity approximated as $\varepsilon = 1 - A = 0.86$. These are median values of the parameters in the distributions derived by Farnocchia et al. (2013b); see Fig. 2 or follow from the solution by Müller et al. (2014). The last parameter, surface thermal conductivity K, was varied in the interval 0.01–1 W/m/K, sufficiently covering all plausible values of the surface thermal inertia Γ between $\simeq 116$ to $\simeq 1150$ (SI units). Note that Müller et al. (2014) report surface inertia values in the 250–800 range (SI units). Their best fit solution of the thermal inertial of 600 (SI units) would correspond to $K \simeq 0.265$ W/m/K in our case. In all solutions we used a timestep $dt = 3$ s and a step $dz = 3 \times 10^{-3}\sqrt{K}$ m at the surface. The lower conductivity K solutions require somewhat smaller step in the depth z, because the penetration depth h_ϕ becomes smaller. Our initial step dz at the surface represents about 1/100 of h_ϕ.

Fig. 1 shows the orbit-averaged value $\langle da/dt\rangle$ for both solutions A and B as function of the surface thermal conductivity K. In fact, the difference between the two solutions is less than 0.1%, so the

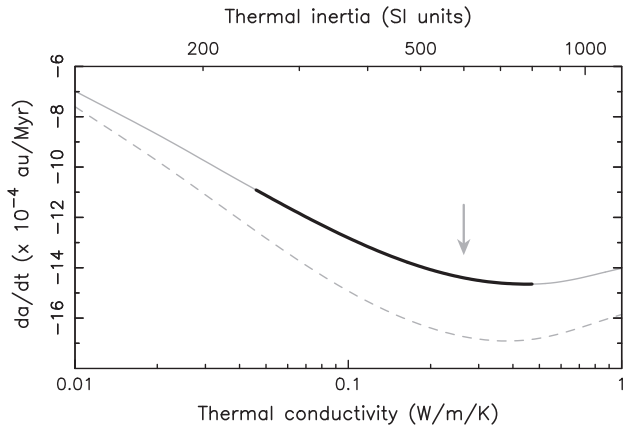

Fig. 1. Secular drift of the orbital semimajor axis $\langle da/dt \rangle$ (averaged over P_{orb} timescale of our solution) due to the Yarkovsky effect for 99942 Apophis (in 10^{-4} au/Myr) as a function of the surface thermal conductivity K (in W/m/K; other physical parameters as in the text). The solid line shows results from our numerical runs for both variants A and B (they both coincide with differences much smaller than the scale of the ordinate). The highlighted black segment shows the $\langle da/dt \rangle$ values that correspond to solutions with the surface thermal inertia between 250 and 800 (SI units) from Müller et al. (2014) (the arrow indicates the thermal inertia value corresponding to the best-fit thermal inertia of 600 in SI units). The dashed line is an analytic approximation valid for a spherical body of size 375 m rotating about a fixed spin axis in the inertial space. The assumed rotation period in this case is $P_\psi P_\phi/(P_\psi - P_\phi) \simeq 30.56$ h and the spin axis direction at ecliptic longitude 250° and latitude −75°, equal to the nominal direction of the rotational angular momentum of the tumbling solution for Apophis (see Pravec et al., 2014).

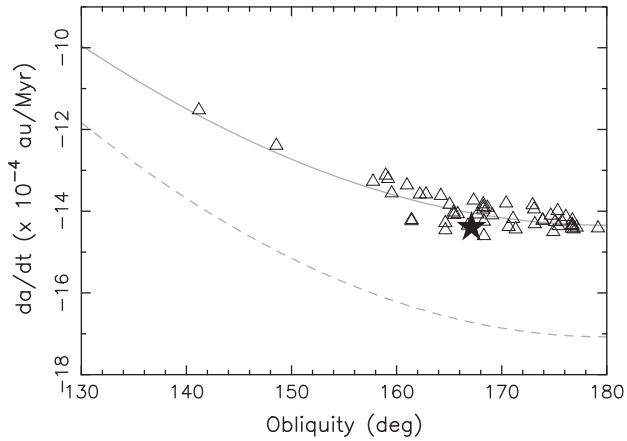

Fig. 2. Secular drift of the orbital semimajor axis $\langle da/dt \rangle$ (averaged over P_{orb} timescale of our solution) due to the Yarkovsky effect for 99942 Apophis (in 10^{-4} au/Myr) as a function of the obliquity γ, defined by the angular distance between the rotational and orbital angular momentum vectors. Open triangles are results from individual runs where the Apophis angular momentum vector was sampling the boundary of its 3σ uncertainty region as in Fig. 4 in Pravec et al. (2014). The star shows the nominal solution of Apophis rotation with obliquity $\simeq 167.1°$. All runs had the nominal value of the surface thermal inertia of 600 (SI units). The dashed line shows the expected $\langle da/dt \rangle \propto \cos\gamma$ dependence from the linear analysis of the Yarkovsky effect for a spherical body. The solid line is the analytic result multiplied by a factor 0.85. The shape and rotation state uncertainties give a ~3% uncertainty in $\langle da/dt \rangle$ for a given obliquity.

two solution entirely overlap at the available resolution of the figure. This is an important justification of our method. The dashed line shows an analytical result from a linearized heat diffusion theory valid for a spherical body in simple rotation on a circular heliocentric orbit (e.g., Vokrouhlický, 1999; Bottke et al., 2006). We assumed a body with 375 m diameter, 30.56 h rotation period and rotation axis directed along the total rotational angular momentum given by Pravec et al. (2014, Table 2). As advocated in Pravec et al. (2014), and confirmed here, such an analytical approximation provides a very good zero approximation for the Yarkovsky effect on Apophis despite its tumbling state. Our numerical solution gives a $\langle da/dt \rangle$ that is about 85% of that obtained with the analytical solution. The reasons for this difference are: (i) non-spherical shape of the body (see Pravec et al., 2014), (ii) non-linearity of the numerical solution, and (iii) non-principal-axis rotation. The dark segment of the solid line shows solutions for which the surface thermal inertia Γ ranges between 250 and 800 (SI units), the interval of values resulting from analysis in Müller et al. (2014). Thanks to the nonlinear dependence of $\langle da/dt \rangle$ on Γ, $\langle da/dt \rangle$ only varies between -15×10^{-4} au/Myr and -11×10^{-4} au/Myr over the Müller et al. (2014) interval for Γ.

The above solutions A and B used the nominal, best-fit solution of Pravec et al. (2014) for the Apophis rotation. However, there is presently a considerable uncertainty in the Apophis rotation solution, see Fig. 4 in Pravec et al. (2014). To test the effect of this uncertainty, we selected 50 solutions from Pravec et al. (2014), all at the 3σ boundary of the angular momentum vector solution (and each individually providing its own shape and other rotation parameters). We reran our Yarkovsky model for each of these rotation models, fixing the value of the surface conductivity at its nominal value 0.265 W/m/K (Müller et al., 2014; other physical parameters as in Fig. 1). In Fig. 2 we plotted the orbit-averaged semimajor axis drift $\langle da/dt \rangle$ as a function of the Apophis "obliquity" angle γ. The latter is approximated by the angular distance between the rotational and orbital angular momentum vectors. The solid line in Fig. 2 shows the expected $\langle da/dt \rangle \propto \cos\gamma$ dependence from the linear analysis of the Yarkovsky effect (e.g., Vokrouhlický, 1999; Vokrouhlický et al., 2000), accounting also for the $\simeq 0.85$ factor mentioned above. We note that the sensitivity of $\langle da/dt \rangle$ to uncertainty in γ is modest because $\gamma \gtrsim 150°$.

2.2. Statistical distribution of semimajor axis change

With the new physical constraints outlined above we could run the previously described Yarkovsky code many times to obtain the statistical distribution of the future Apophis position. We think this high-accuracy approach will eventually become imperative as the parameter space of the Yarkovsky effect is more and more constrained, and in particular when the effect is unambiguously detected (see Section 3). With that approach it will be important to ensure that the computed accelerations are consistent with the asteroid's actual heliocentric orbit as it evolves under close planetary encounters.

For the present we instead employ a simpler method that uses the approach outlined in Farnocchia et al. (2013b). What we need first is a statistical distribution of the current mean semimajor axis drift $\langle da/dt \rangle$ for Apophis, and from this we derive the distribution of a proxy transverse acceleration that fully captures the salient effects of the thermal recoil acceleration. As we discuss briefly below and as described in detail by Farnocchia et al. (2013b), this transverse acceleration is modeled through usual the nongravitational acceleration parameter A_2, which depends only on the asteroids physical and spin characteristics and does not have a significant dependence on the object's semimajor axis and eccentricity. Here we derive the distribution of $\langle da/dt \rangle$, and in the following section we use that to obtain the distribution in A_2.

The important message from the tests presented above is that we may use a simple analytical formula for the diurnal effect from Vokrouhlický (1999), valid for a spherical body rotating about the fixed spin axis in space, multiplied by the correction factor $f = 0.85$ for the non-sphericity and non-linearity effects,[3] to obtain the

[3] Note that this value replaces the guessed correction factor $f = 0.7$ in Section 4.1 of Pravec et al. (2014).

needed information. This is similar to what has been used in Pravec et al. (2014), but we use here proper correlations among the parameters from Müller et al. (2014). In particular, the assumed values of obliquity are those derived for the rotational angular momentum vector in Fig. 7 (left panel) of Pravec et al. (2014). In order to compute $\langle da/dt \rangle$ we need to set the values of (i) the effective size D, (ii) thermal inertia Γ, and (iii) Bond albedo A. These are taken from Müller et al. (2014) distributions that provide also a full correlation analysis between these parameters (see also Müller and Lagerros (1998, 2002) for tests and validation of the thermal model).

One other key parameter is the asteroid's bulk density. This last parameter has not been constrained by either of the two papers used above. Our nominal guess of 2 g/cm^3 assumed above was based on the the density value derived for other S-type asteroids of a comparable size: (i) the $\simeq$1 km size asteroid (5381) Sekhmed (e.g., Neish et al., 2003), (ii) the $\simeq$1.1 km size asteroid (35107) 1991 VH (e.g., Carry, 2012), (iii) the $\simeq$0.4 km size asteroid (25143) Itokawa (e.g., Fujiwara et al., 2006; Abe et al., 2006), and (iv) the $\simeq$1.3 km size asteroid (66391) 1999 KW4 (e.g., Ostro et al., 2006). Note, however, that the $\simeq$0.45 km satellite of the latter has a bulk density of $\simeq$2.8 g/cm^3, reflecting lower macroporosity than the primary component in this binary system. Additionally, Lowry et al. (2014) analysed implications of the detected YORP effect for Itokawa by using a detailed thermophysical model and concluded that the asteroid consists of two very different parts: (i) the main body with the density $\simeq$1.75 g/cm^3 and (ii) the head with the density $\simeq$2.85 g/cm^3. While this striking difference may be in part due to their model incompleteness (e.g., Golubov et al., 2014; Ševeček et al., 2015), the two values again roughly bracket the expected interval of Apophis bulk density. We thus use the same bulk-density distribution function as shown in Fig. 2 of Farnocchia et al. (2013b), which is based on Binzel et al. (2009).

Rozitis and Green (2012) showed the Yarkovsky effect is always enhanced by the effect of surface unresolved roughness. Since we do not have surface roughness information for Apophis, we take an approach analogous to that adopted by Chesley et al. (2014), see Fig. 10 for asteroid (101955) Bennu. Specifically, we scaled $\langle da/dt \rangle$ by a surface roughness enhancement factor that, for the Apophis thermal inertia range, increases the semimajor axis drift by a value as large as 20%. Given a value of the thermal inertia, the maximum estimated factor has served to define a template interval. Without more detailed information, we considered median enhancement to be half of this maximum factor with a Gaussian distribution reaching limits of the interval at the 3σ significance level.

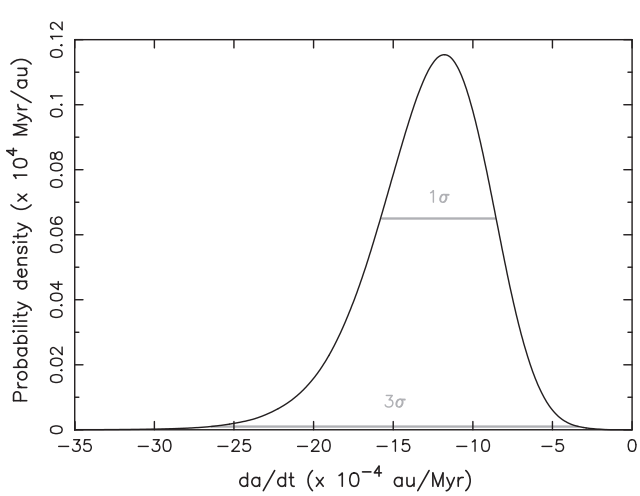

Fig. 3. Statistical distribution of $\langle da/dt \rangle$ obtained from the theoretical modeling with parameters described in the text. The gray horizontal bars correspond to 1σ and 3σ intervals.

Finally, we need to account for the uncertainties of the Pravec et al. (2014) shape and rotation models. As shown by Fig. 2, and further tested by clone variants of Apophis having slightly different shape, these uncertainties map into a $\sim$3% dispersion in $\langle da/dt \rangle$ (formal 1σ value). Therefore, we added a 3% random noise to the sampled $\langle da/dt \rangle$.

The distribution of $\langle da/dt \rangle$ computed according to the parameter distributions described above has a mean of -12.8×10^{-4} au/Myr and a formal standard deviation of 3.6×10^{-4} au/Myr. Fig. 3 shows the corresponding $\langle da/dt \rangle$ distribution, which is actually not symmetric around its peak $\langle da/dt \rangle = -11.8 \times 10^{-4}$ au/Myr. As a matter of fact, the median value is -12.4×10^{-4} au/Myr, the 1σ interval spans from -15.7×10^{-4} au/Myr to -8.6×10^{-4} au/Myr, and the 3σ interval from -26.4×10^{-4} au/Myr to -3.4×10^{-4} au/Myr.

3. Implications on the trajectory and impact hazard

Chesley (2006), Giorgini et al. (2008), and Farnocchia et al. (2013b) prove that the Yarkovsky effect is the main source of uncertainty for the Apophis ephemeris prediction. As an example, for the gravity-only orbital solution the formal 3σ uncertainty of the time of closest approach in 2029 is about 1 s. On the other hand, the Yarkovsky effect can change the time of closest approach by tens of seconds.[4]

To account for the Yarkovsky accelerations, we added a tangential acceleration $A_2\,(1\,\mathrm{au}/r)^2$ to the force model (Farnocchia et al., 2013a). One way to constrain A_2 is to use the fit to the astrometric observations. We selected the most reliable optical astrometry available for Apophis through February 26, 2014, namely observations by Tholen et al. (2013), and MPEC 2014-R71, Pan-STARRS PS1, and Magdalena Ridge Observatory. Moreover, we included thirteen delay and seven Doppler radar observations,[5] including the ones from the most recent radar apparition of late 2012 and early 2013. By using the Farnocchia et al. (2015) statistical treatment for the optical astrometry as well as some ad hoc weights (see Farnocchia et al. (2013b) for details) we obtain $A_2 = (-51 \pm 28) \times 10^{-15}$ au/d^2, which is a notable indication, but only a marginal detection, of the Yarkovsky effect.

Another way to constraint A_2 is to use the physical model of Apophis. The semimajor axis drift distribution obtained in Section 2.2 can be converted to A_2 as (see Farnocchia et al., 2013a):

$$A_2 = \frac{1}{2}\, n \left(\frac{a}{1\,\mathrm{au}}\right)^2 (1 - e^2) \left(\frac{da}{dt}\right), \tag{1}$$

where e and a are the eccentricity and semimajor axis assumed in Section 2, and n the orbital mean motion.

Fig. 4 shows the A_2 distribution obtained from the astrometry and that obtained from the physical model. The figure also shows the A_2 distribution obtained by combining the independent information coming from both astrometry and physical model. It is worth noticing that, since the constraint from the astrometry is weak, the combined distribution is close to that coming from the physical model only.

We now use the combined distribution of A_2 to make ephemeris predictions. In particular, we want to assess the implications on the Earth impact hazard. As already discussed in full detail by

[4] See also Žižka and Vokrouhlický (2011) for a discussion of a smaller effect of the direct radiation pressure and pressure of the sunlight scattered by the asteroid surface. Altogether, these effects would produce orbital perturbation amounting to about few percent of that due to the Yarkovsky effect. For that reason we neglect them in the present study.

[5] http://ssd.jpl.nasa.gov/?radar.

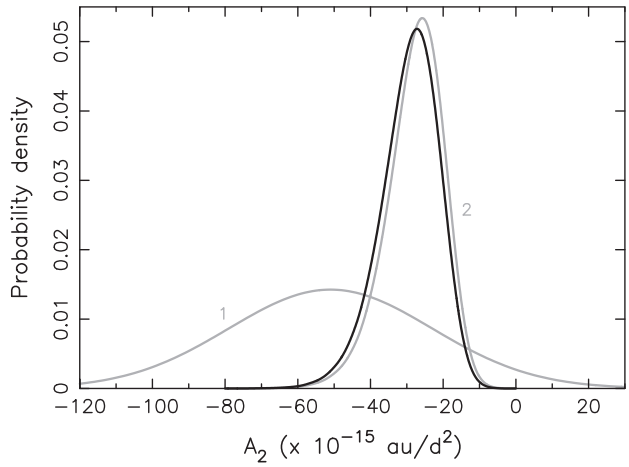

Fig. 4. Probability density distribution (ordinate) of the A_2 transverse acceleration parameter: (i) from the Apophis orbital fit using the currently available optical and radar astrometry (gray curve labeled 1), (ii) from the theoretical modeling with parameter distributions described in the text (gray curve labeled 2), and (iii) resulting combination of (i) and (ii) shown by the black solid line.

Farnocchia et al. (2013b), this analysis is best performed on the 2029 *b*-plane, i.e., the plane including the geocenter and normal to the incoming asymptote of the Apophis trajectory with respect to the Earth during the 2029 encounter (Valsecchi et al., 2003). The coordinates $(\xi_{2029}, \zeta_{2029})$ on the *b*-plane are defined so that the projection of the Earth's heliocentric velocity onto the *b*-plane defines the negative ζ_{2029}-axis. Thus, the ζ_{2029} coordinate defines how early or late Apophis for the minimum possible encounter distance with the Earth. Because of Keplerian motion the orbital uncertainties stretch into a slender ellipsoid along the orbit. The Yarkovsky effect is the largest to affect the along-track position since the semimajor axis drift causes an along-track runoff that accumulates quadratically with time. Since the along-track uncertainty is strictly related to the time uncertainty, it is convenient to parameterize the projection of the orbital uncertainty by using the ζ_{2029} coordinate (for more details see Farnocchia et al., 2013b).

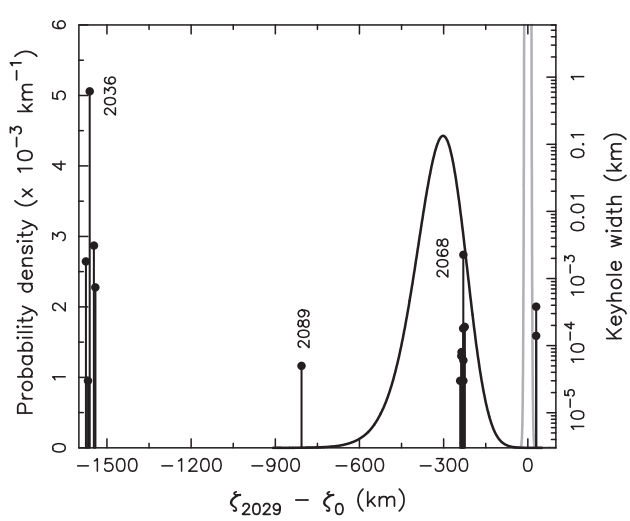

Fig. 5. The gray curve shows the probability density function of ζ_{2029} for a gravity-only orbital solution, with the origin arbitrarily shifted to zero at the nominal value $\zeta_0 = 47,677$ km. The peak of this distribution is 0.07 km^{-1} and is therefore outside the vertical range of the plot. The black curve shows the probability density function of ζ_{2029} obtained including the Yarkovsky effect in the model. The vertical bars correspond to the keyholes and their height is proportional to the keyhole width. The impact probabilities can be computed as the product of the ζ_{2029} density function and the keyhole widths.

Table 1
Possible Earth impacts for Apophis. Columns are impact epoch, 2029 keyhole location and width, probability density function (PDF) of $\zeta_{2029} - \zeta_0$ at the keyhole, and impact probability (IP). Here $\zeta_0 = 47,677$ km is an arbitrary point of reference, as depicted in Fig. 5. Only the impacts with probability greater than 10^{-7} are shown.

Date TDB	$\zeta_{2029} - \zeta_0$ km	Width m	PDF 10^{-3} km^{-1}	IP 10^{-6}
2060-04-12.6	−241	0.03	3.3	0.1
2065-04-11.8	−237	0.08	3.2	0.3
2068-04-12.6	−230	2.25	3.0	6.7
2076-04-13.0	−224	0.19	2.8	0.5
2077-04-13.5	−230	0.06	3.0	0.2
2078-04-13.8	−236	0.07	3.2	0.2
2091-04-13.4	−236	0.07	3.2	0.2
2103-04-14.4	−230	0.18	3.0	0.5

Fig. 5 shows the distribution of ζ_{2029} for both a gravity-only solution and the one accounting for the Yarkovsky effect. The statistically significant difference between the two predictions is evident: the gravity-only prediction is $\zeta_{2029} = (47,677 \pm 6)$ km, while the solution including the Yarkovsky effect yields $\zeta_{2029} = (47,354 \pm 90)$ km. It is worth noticing how the inclusion of the Yarkovsky effect produces a ~ 300 km shift in the nominal prediction and increases the uncertainty by more than a factor of ten. The mean value and width of the distribution function accounting for the Yarkovsky effect mostly depends on the obliquity, size and thermal inertia, and bulk density constraints. Overall it would shift toward smaller ζ_{2029} values for smaller obliquity, larger size or smaller surface thermal inertia, and larger bulk density (and vice versa).

To obtain the hazard assessment we use the keyholes on the 2029 *b*-plane, namely the regions on the 2029 *b*-plane leading to an impact at a later encounter (e.g., Chodas, 1999). The 2029 keyholes have already been computed in Farnocchia et al. (2013b) and are shown, along with their widths, in Fig. 5. To compute the probability of an impact during one of the post-2029 encounters, all we have to do is integrate the ζ_{2029} probability density function over the corresponding keyhole. Table 1 reports all the possible impacts with impact probability greater than 10^{-7}. The highest risk encounter is that of April 2068 with an impact probability of seven in a million.

Since the rotation state of Apophis could change during the 2029 encounter (Scheeres et al., 2005), the post-2029 trajectory cannot be exactly known until the post-2029 rotation state is determined. As a consequence, the exact location of the keyholes depends on the post-2029 Yarkovsky effect, unknown to us at the moment. Luckily, as already discussed in Farnocchia et al. (2013b), whatever post-2029 strength of the Yarkovsky effect, the keyhole structure can only change slightly: they can shift by up to $\simeq$0.5 km without significantly changing their width. Therefore, the current impact probability computations are not significantly affected by this unknown aspect of Apophis dynamics.

4. Conclusions

We performed a detailed numerical determination of the Yarkovsky effect for potentially hazardous asteroid 99942 Apophis. To that goal we used the up-to-date information of this body's rotation state and its surface thermal inertia. The currently unconstrained parameters of the model were simulated using a Monte Carlo scheme from other asteroid analogs. We also collected the currently available astrometric dataset, both optical and radar measurements, of this asteroid. Our orbit determination provides a low-SNR indication of the Yarkovsky effect from the astrometry fit.

As already anticipated in Pravec et al. (2014), our solution modifies the impact probabilities of Apophis given by Farnocchia et al. (2013b) in two ways: (i) first, some impact possibilities were eliminated or their probability became negligible, and (ii) second, the composite impact probability increased by a factor of about three. Both are principally due to the constrained spin solution for Apophis. Thus the impact possibilities that were related to prograde rotation state of Apophis in Farnocchia et al. (2013b) analysis have now effectively null probability. On the other hand, those that reside near the confirmed retrograde spin state of Apophis reveal slightly larger impact probability. This concerns a cluster of resonant return solutions in the 2029 *b*-plane led by the April 12.6, 2068 Earth impact solution.

As discussed in Farnocchia et al. (2013b), the next favorable observational window of Apophis starts in November 2020 and extends through spring and summer of 2021, when high quality radar measurements could be taken. If successful, these observations will certainly help shrink the current astrometric constraint of the Yarkovsky effect from SNR of about 1.8 to a value near or larger than 10. At that moment, the fate of the Apophis orbit for the future century will be much better known. Interestingly, the role of astrometry and modeling as far as the Yarkovsky effect is concerned will likely interchange. Fig. 4 indicates that currently the broad Yarkovsky constraint comes basically from the model side with virtually no astrometric contribution. After 2020/2021 observational campaign, the astrometric determination of the Yarkovsky effect will likely overwhelm the modeling part. This is actually desirable, because such a constraint is less dependent on model assumptions and parameters. However, the approach to the Earth in March 2021 will also offer a possibility for a wealth of photometric observations both in the optical and thermal wavebands. These could serve to refine the currently coarse constraints on the rotation state and thermal inertia of this body. If combined with the astrometric value of the Yarkovsky effect, such data may help determine the bulk density of Apophis with the approach demonstrated by Chesley et al. (2014), who used the Yarkovsky effect to obtain a density constraint for asteroid (101955) Bennu. Such information will also be very important if the impact possibilities persist.

Acknowledgements

We thank the anonymous referees for suggestions that helped to improve the original version of this paper. This work was supported by the Czech Grant Agency (Grants P209/12/0229 and P209-13-01308S). D. Farnocchia and S.R. Chesley conducted this research at the Jet Propulsion Laboratory, California Institute of Technology, under a contract with the National Aeronautics and Space Administration.

References

Abe, S. et al., 2006. Mass and local topography measurements of Itokawa by Hayabusa. Science 312, 1344–1347.
Binzel, R.P. et al., 2009. Spectral properties and composition of potentially hazardous asteroid (99942) Apophis. Icarus 200, 480–485.
Bottke, W.F. et al., 2006. The Yarkovsky and Yorp effects: Implications for asteroid dynamics. Annu. Rev. Earth Planet. Sci. 34, 157–191.
Breiter, S., Rożek, A., Vokrouhlický, D., 2011. YORP effect on tumbling objects. Mon. Not. R. Astron. Soc. 417, 2478–2499.
Brown, R.H., Matson, D.L., 1987. Thermal effects of insolation propagation into the regoliths of airless bodies. Icarus 72, 84–94.
Čapek, D., 2006. Thermal Effects in Physics and Dynamics of Small Bodies of the Solar System, Ph.D. Thesis. Charles Univesity, Prague.
Čapek, D., Vokrouhlický, D., 2005. Accurate model for the Yarkovsky effect. In: Knežević, Z., Milani, A. (Eds.), Dynamics of Populations of Planetary Systems. Cambridge University Press, Cambridge, pp. 171–178.
Carry, B., 2012. Density of asteroids. Planet. Space Sci. 73, 98–118.
Chesley, S.R., 2006. Potential impact detection for near-Earth asteroids: The case of 99942 Apophis (2004 MN4). In: Lazzaro, D., Ferraz-Mello, S., Fernández, J. (Eds.), Asteroids, Comets, Meteors. Cambridge University Press, Cambridge, pp. 215–228.
Chesley, S.R. et al., 2014. Orbit and bulk density of the OSIRIS-REx target Asteroid (101955) Bennu. Icarus 235, 5–22.
Chesley, S.R., et al., 2009. An updated assessment of the impact threat from 99942 Apophis. In: DPS Meeting 41. Abstract 43.06.
Chesley, S.R., Baer, J., Monet, D.G., 2010. Treatment of star catalog biases in asteroid astrometric observations. Icarus 210, 158–181.
Chodas, P.W., 1999. Orbit uncertainties, keyholes, and collision probabilities. Bull. Am. Astron. Soc. 31, 1117.
Farnocchia, D., Chesley, S.R., 2014. Assessment of the 2880 impact threat from Asteroid (29075) 1950 DA. Icarus 229, 321–327.
Farnocchia, D. et al., 2013a. Near Earth asteroids with measurable Yarkovsky effect. Icarus 224, 1–13.
Farnocchia, D. et al., 2013b. Yarkovsky-driven impact risk analysis for Asteroid (99942) Apophis. Icarus 224, 192–200.
Farnocchia, D. et al., 2015. Star catalog position and proper motion corrections in asteroid astrometry. Icarus 245, 94–111.
Fujiwara, A. et al., 2006. The rubble-pile asteroid Itokawa as observed by Hayabusa. Science 312, 1330–1334.
Giorgini, J.D. et al., 2002. Asteroid 1950 DA's encounter with Earth in 2880: Physical limits of collision probability prediction. Science 296, 132–136.
Giorgini, J.D. et al., 2008. Predicting the Earth encounters of (99942) Apophis. Icarus 193, 1–19.
Golubov, O., Krugly, Y.N., 2012. Tangential component of the YORP effect. Astrophys. J. 752, L11 (5pp.).
Golubov, O. Scheeres, D.J., Krugly, Y.N., 2014. A three dimensional model of tangential YORP. Astrophys. J. 794, 22 (9pp.).
Kaasalainen, M., 2001. Interpretation of lightcurves of precessing asteroids. Astron. Astrophys. 376, 302–309.
Landau, L.D., Lifschitz, E.M., 1960. Mechanics. Addison-Wesley, Reading.
Lowry, S.C. et al., 2014. The internal structure of asteroid (25143) Itokawa as revealed by detection of YORP spin-up. Astron. Astrophys. A48 (9pp.).
Milani, A. et al., 2009. Long term impact risk for (101955) 1999 RQ36. Icarus 203, 460–471.
Müller, T.G., Lagerros, J.S.V., 1998. Asteroids as IR standards for ISOPHOT. Astron. Astrophys. 338, 340–352.
Müller, T.G., Lagerros, J.S.V., 2002. Asteroids as calibration standards in the thermal infrared for space observatories. Astron. Astrophys. 381, 324–339.
Müller, T.G. et al., 2014. Thermal infrared observations of Asteroid (99942) Apophis with Herschel. Astron. Astrophys. 566, A22 (10pp.).
Neish, C.D. et al., 2003. Radar observations of binary asteroid 5381 Sekhmet. Bull. Am. Astron. Soc. 35, 1421.
Ostro, S.J. et al., 2006. Radar imaging of binary near-Earth asteroid (66391) 1999 KW4. Science 314, 1276–1280.
Pravec, P. et al., 2005. Tumbling asteroids. Icarus 173, 108–131.
Pravec, P. et al., 2014. The tumbling spin state of (99942) Apophis. Icarus 233, 48–60.
Rozitis, B., Green, S.F., 2012. The influence of rough surface thermal-infrared beaming on the Yarkovsky and YORP effects. Mon. Not. R. Astron. Soc. 423, 367–388.
Rozitis, B., Green, S.F., 2013. The influence of global self-heating on the Yarkovsky and YORP effects. Mon. Not. R. Astron. Soc. 433, 603–621.
Scheeres, D.J. et al., 2005. Abrupt alteration of Asteroid 2004 MN4's spin state during its 2029 Earth flyby. Icarus 178, 281–283.
Ševeček, P., et al., 2015. The thermal emission from boulders on (25143) Itokawa and general implications for the YORP effect. Mon. Not. R. Astron. Soc. (in press).
Spoto, F. et al., 2014. Non-gravitational perturbations and virtual impactors: The case of asteroid (410777) 2009 FD. Astron. Astrophys. A100 (8pp.).
Tholen, D.J., Micheli, M., Elliott, G.T., 2013. Improved astrometry of (99942) Apophis. Acta Astron. 90, 56–71.
Valsecchi, G.B. et al., 2003. Resonant returns to close approaches: Analytical theory. Astron. Astrophys. 408, 1179–1196.
Vokrouhlický, D., 1999. A complete linear model for the Yarkovsky thermal force on spherical asteroid fragments. Astron. Astrophys. 344, 362–366.
Vokrouhlický, D., Chesley, S.R., Milani, A., 2000. Yarkovsky effect on near-Earth asteroids: Mathematical formulation and examples. Icarus 148, 118–138.
Vokrouhlický, D. et al., 2005. Yarkovsky detection opportunities. I. Solitary asteroids. Icarus 173, 166–184.
Vokrouhlický, D. et al., in press. The Yarkovsky and YORP effects. In: Michel, P., DeMeo, F.E., Bottke, W.F. (Eds.), Asteroids IV. University of Arizona Press, Tucson (in press).
Žižka, J., Vokrouhlický, D., 2011. Solar radiation pressure on (99942) Apophis. Icarus 211, 511–518.